STUDY OF Mn INTERSTITIALS IN (Ga,Mn)As USING HRXRD

L. Horák[1], J. Matějová[1], X. Martí[1], V. Holý[1], V. Novák[2], Z. Šobáň[2,3], S. Mangold[4], and F. Jimenez-Villacorta[5]

[1]*Department of Condensed Matter Physics, Charles University, Prague, Czech Republic*
[2]*Institute of Physics ASCR, Prague, Czech Republic*
[3]*Department of Microelectronics, The Czech Technical University in Prague, Czech Republic*
[4]*Karlsruhe Institute of Technology, Karlsruhe, Germany*
[5]*Department of Chemical Engineering, Northeastern University, Boston, USA*
horak@karlov.mff.cuni.cz

Keywords:
(Ga,Mn)As, thin layers, interstitials, diffusion

Abstract

A method for the determination of the concentration depth profiles of Mn interstitial ions in (Ga,Mn)As thin epitaxial layers using high-resolution x-ray diffraction (HRXRD) is presented. The structure factor is affected by the presence of antisite defects and Mn ions in nonequivalent lattice positions, their particular influence on the structure factor differs for various Miller indices *hkl*. The diffraction curves were measured for several diffraction maxima *hkl* and they were fitted by the theoretical curves. The depth profiles of the Mn interstitial density obtained for the sample in various annealing states were compared to the numerical drift-diffusion simulations, from this comparison the diffusivity of the interstitials in (Ga,Mn)As host lattice has been estimated.

Introduction

The (Ga,Mn)As, belonging to the diluted magnetic semiconductors, is intended for a spintronics application. Magnetic Mn ions are diluted in a semiconductor GaAs host lattice, ideally, they substitute Ga atoms and they (being acceptors) provide the semiconductors by the holes. The mutual interaction between relatively distant Mn ions is mediated just by these holes [1]. The thin (Ga,Mn)As layers are usually prepared by molecular beam epitaxy (MBE). In order to prevent the formation of MnAs inclusions, the growth temperature has to be lower than it is usual for the GaAs growth. Due to this low-temperature growth many defects are present in the prepared material. Firstly, there are many As atoms sitting in Ga positions (so called anti-site defects). Secondly, Mn ions are present also in interstitial positions. Both defects act in semiconductor as double-donors, which decrease the concentration of holes and consequently decrease the Curie temperature [2]. The amount of the interstitials can be reduced by the post-growth annealing (temperature around 200 °C) [2], which leads to the out-diffusion of the interstitials to the free surface. The substitutional Mn and anti-site defects are expected to be immobile at these temperatures and they are not affected by the annealing. The decrease of the interstitial density improve magnetic properties of the Ga(MnAs). Although this material has been intensively studied for the last decade, the process of the out-diffusion is not fully understood yet and there are only few estimations of Mn diffusivity in the literature [2–3].

Theory of diffraction

The Mn atoms can substitute Ga atoms in the GaAs zinc-blende structure (the occupancy denoted as $c_{\mathrm{Mn(sub)}}$, or they can occupy two non-equivalent interstitial positions in the centres of the Ga and the As tetrahedrons (figure 1), we denote these interstitial positions as **TGa** and **TAs**, respectively. There are also many arsenic *anti-site* defects (Ga atom substituted by the arsenic ones with occupancy c_{anti}) due to the low temperature growth. The average structure factor for (Ga,Mn)As

$$\begin{aligned}\left\langle F_{hkl}^{(Ga,Mn)As}\right\rangle \quad & F_{hkl}^{GaAs} \quad 4c_{anti}\,(f_{As} \quad f_{Ga}) \\ & 4c_{Mn(sub)}\,(f_{Mn} \quad f_{Ga}) \\ & 4c_{Mn(TAs)}\,f_{Mn}\exp(i\ (h \quad k \quad l)) \\ & 4c_{Mn(TGa)}\,f_{Mn}\exp(\ \ i\ /2(h \quad k \quad l))\end{aligned} \tag{1}$$

for the Miller indices *hkl* can be derived from the GaAs structure factor (1st term) including contributions from the presence of the antisite defects (2nd term) and the Mn ions in substitutional (3rd term) and interstitial positions (4th and 5th term for TAs, resp. TGa). The atomic scattering factors are denoted as *f*, the concentrations of the defects as *c*, both subscripted intuitively. It is obvious, that the difference between the atomic scattering factors of Ga and Mn (resp. As) is too small to determine the number of substituted Ga atoms reliably. This can be partially solved using the assumption that the number of the substituted Ga atoms is not affected by the annealing.

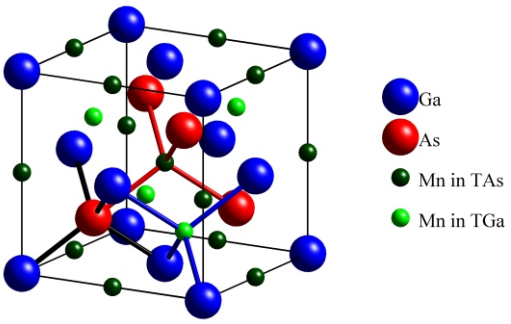

Figure 1. Sketch of the unit cell of zinc-blend (Ga,Mn)As. The Ga atom can be substituted by the Mn or by the As anti-site atom. Possible interstitials are located in the centres of the Ga (or As) tetrahedrons.

From the theoretic calculations in [4], it follows that the lattice is locally distorted around the interstitials. It is possible to include this distortion effect to the structure factor very easily if we can assume the random positions of the interstitials and their low concentration. As only the closest neighbourhood is affected by the presence of the interstitials (very weak defect), the structure factor is averaged over the statistical ensemble of all configurations of the distorted and the undistorted unit cells. Details can be found in [5].

The dependence of the structure factor and consequently the dependence of the intensity on the Mn concentration at the mentioned nonequivalent lattice positions differs for different *hkl* due to the phase terms in Eq. 1. The change of the structure factor with the substitutional content is very low, whereas the intensity strongly depends on the number of interstitials in the TAs and the TGa positions. It is necessary to measure diffraction curves around several diffraction maxima to determine the interstitial concentration reliably. All three types of maxima with different phase term in Eq. 1 should be included in measured set of diffractions (fulfilling for strong ($N = 0$), intermediate ($N = 1, 3$) and weak ($N = 2$)). The Debye-Waller factor (DWF) including thermal vibrations and static disorder also affects the intensity; to avoid this correlation one should measure more diffractions in a wide range of diffraction angles. The optimum set of diffraction for laboratory measurement we found as (002), (004), (115) with an additional intermediate diffraction, e.g., (113) or (117). The figure 2 shows the dependence of the diffracted intensity on the Mn concentrations (restricted only to Mn content) and it illustrates how the parameters representing the concentrations correlate in a fitting procedure.

We assume that the concentration of the antisite defects and the substitutional Mn are the same for all annealing states of the samples as only the interstitial concentration changes during the annealing. To avoid a correlation between many parameters (antisite defects density, Mn density in three nonequivalent positions) all measured data have to be fitted simultaneously sharing the parameters not affected by the annealing ($c_{Mn(sub)}$, c_{anti}). The expansion coefficients from [6] were taken into account to compute the relaxed lattice parameter of (Ga,Mn)As, which is affected by the presence of the anti-sites and the Mn in substitutional and interstitial positions. Although the precision of estimated expansion coefficients is very low, using them as free parameters helped a lot to stabilize numerical fitting procedure.

Theory of diffusion

Taking into account the movement of the Mn ions in the surroundings of charged holes, we simulate the redistribution of Mn interstitials with the local density n during the annealing by the solution of the drift-diffusion equation for interstitials in one dimension [7]:

$$\frac{dn}{dt} \quad \frac{d}{dz} \; D_n \frac{dn}{dz} \quad {}_n n \frac{d}{dz} \quad \frac{d}{dz} \quad j_n \;, \qquad (2)$$

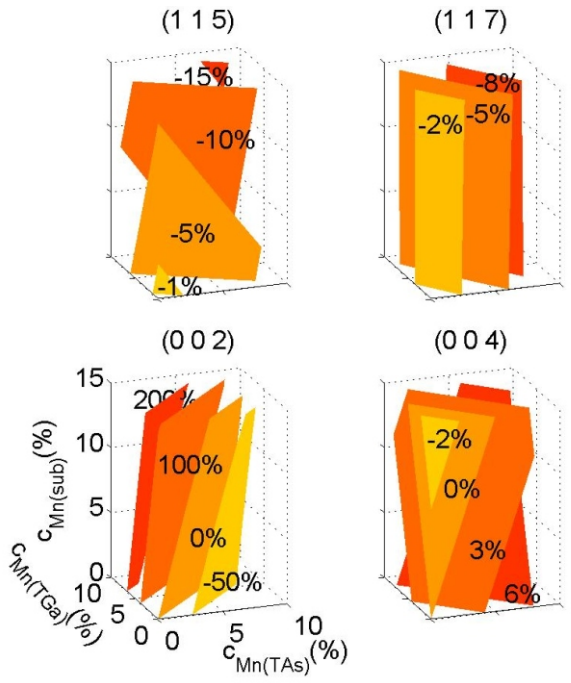

Figure 2. The distribution of the calculated intensity in the 3D space on Mn concentrations. Each point represents the intensity for the corresponding concentrations of Mn in all considered lattice positions. Only a few iso-intensity surfaces are plotted for clarity for each diffraction. The numbers within the planes indicate the intensity change with respect to the intensity of pure GaAs. The distributions of intensity are plotted for weak diffraction maximum (002), strong (004) and two intermediate diffraction maxima (115) and (117).

where D_n is the diffusivity and μ_n mobility of the interstitials connected by the Einstein relation. A quantity j_n corresponds to the flux of the interstitials. Here we do not distinguish between the different non-equivalent interstitial positions, therefore *n(z)* should be compared to $c_{Mn(TAs)} + c_{Mn(TGa)}$. Of course, not only the interstitials are mobile, their movement is followed by the hole flux to screen the charge of the interstitials, and the change of the hole density p can be described similarly

$$\frac{dp}{dt} \quad \frac{d}{dz} \; D_p \frac{dp}{dz} \quad {}_p p \frac{d}{dz} \quad \frac{d}{dz} \quad j_p \qquad (3)$$

The electric field is represented by electrostatic potential , the Poisson equation for the potential

$$\frac{d^2}{dz^2} \quad (c_{Mn(sub)} \quad p \quad 2n) \frac{e}{} \qquad (4)$$

completes the system of the drift-diffusion equations. The constant e is the elementary charge and stands for the permittivity of the material (GaAs). Additional terms for charged particles can be included, such as the anti-site defects, if they are present.

The boundary conditions for the electric field (in Eq. 4) satisfy the requirement to have negligible electric intensity deep in the substrate (first derivative of potential equal to

zero at coordinates corresponding to the bottom of the substrate), the value of the electric potential at the surface is arbitrary as only its derivative is relevant. Also the fluxes of the interstitials and the holes are zero deep in the substrate ($j_n = 0$ and $j_p = 0$ at the bottom of the substrate). On the other hand, Mn atoms in the interstitial positions near the surface are oxidized by ambient oxygen diffusing to the lattice. This mechanism is responsible for the passivation of the interstitials below the surface [8]. We do not model the in-diffusion and chemical reactions of the oxygen, we simplify the simulation by considering a model surface container, which traps interstitials until it is full (saturated). The rate of the trapping is decreased as the container is being filled. Then interstitials near the surface (at coordinate $\mathbf{z}_{surface}$) flows out from our system to this container. Regarding this requirements the flux to the container (which is actually the boundary condition at the surface) can be defined as

$$j_{n/\,surface}(t) \quad S_0 \; 1 \; \frac{N(t)}{N_{\max}} \; n(t, z \quad z_{surface}). \qquad (5)$$

S_0 is the trapping rate of the container, phenomenological quantity related to the oxygen diffusion and the rate of the chemical reaction. $N(t)$ is the actual filling of the container, while the N_{max} is its capacity. Each removed (oxidized) interstitial ion (double-donor) from the system is replaced by two released holes ($j_{p|\text{surface}} = 2\, j_{n|\text{surface}}$).

The more extensive discussion is beyond of the scope of the extended abstract, the further details can be found in [9].

Experimental details

The epitaxial GaMnAs layers under the study were grown on (001)GaAs substrates by the molecular beam epitaxy. The nominal thickness was 100 nm and the intended doping was 14 % of manganese (for clarity, the atomic ratio Mn/Ga was expected to be 14/86). A nondestructive character of the characterization (in contrast for instance to the transmission electron microscopy) allows to investigate the same sample in various annealing states, i.e., to measure diffraction curves around several diffraction maxima *hkl*. We measured an as-grown sample, then after 24 hours of annealing in the air at 160°C and finally after 20 cycles of etching and short annealing (under the same conditions as in the previous case). The etching procedure was performed in order to remove the oxidized surface layer, which inhibits the out-diffusion of interstitials.

The measured diffraction curves for several diffraction maxima *hkl* were fitted to the theoretical curves based on standard dynamical diffraction theory [10]. The figure 3 shows the measured data with their fits. All diffraction curves were fitted simultaneously using shared parameters ($c_{Mn(sub)}$, c_{anti}) for different annealed states. For each annealing state individual parameters (layer thickness, DWF, $_{c}Mn(TGa)$ and $c_{Mn(TAs)}$) were optimized.

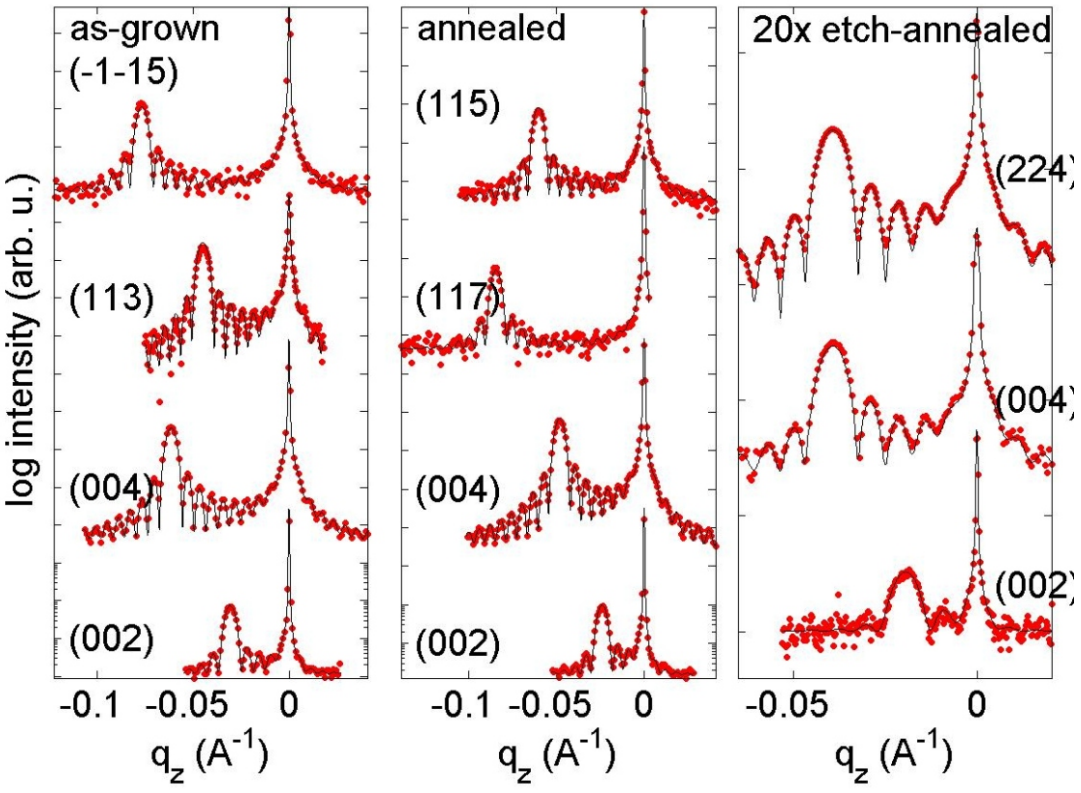

Figure 3. The measured diffraction curves (red circles) for as-grown, annealed and re-annealed (sequentially 20x etched and annealed) sample with their theoretical fits (black solid line).

Results

As we showed above, the sensitivity to the Mn content in substitutional positions is very small (the error would be much larger than the value itself), but this quantity and the anti-site defect density correlate to the concentration of the interstitials. We ran our fitting procedure for large set of fixed values of $c_{Mn(sub)}$ and c_{anti} with the requirement that the calculated lattice parameter has to reflect the measured position of the layer peak. We obtained optimized values of two particular concentrations of interstitials for many pairs of such fixed parameters. From our later analysis it follows that the anti-site defect density is very low (below 1%), because only for that small c_{anti} it was possible to reach the best fit of the measured data and the simulated curves. The figure 4 shows the correlation of the concentrations of the Mn in interstitial positions and the substitutional positions. As our method is not able to determine the $c_{Mn(sub)}$ separately, only from this analysis it is not possible to determine all parameters due to this correlation.

There are no reports on the successful growth of the (Ga,Mn)As samples with higher concentration of substitutional Mn than 9% in the literature. Transport measurements showed that the as-grown sample is very compensated, recalling the intended doping value it allowed us to estimate the substitutional Mn content to 8 % – 9 %. This estimation was confirmed by anomalous x-ray diffraction on performed on the same samples at the photon energy around the Mn *K* absorption edge ($c_{Mn(sub)} = (8.2 \pm 1.1)\%$) [11]. These results indicate that for higher flux of Mn atoms during the growth the generation of the anti-site defects is rather suppressed and the higher density of the Mn interstitials occurs. Moreover, even this very roughly estimated Mn content in substitutional positions allows to determine the concentration of the interstitials using the graph in figure 4. For the later drift-diffusion simulations only the quantity $c_{Mn(TAs)} + c_{Mn(TGa)}$ is important, which is nearly independent on actual value of $c_{Mn(sub)}$ as it follows from the Fig. 4.

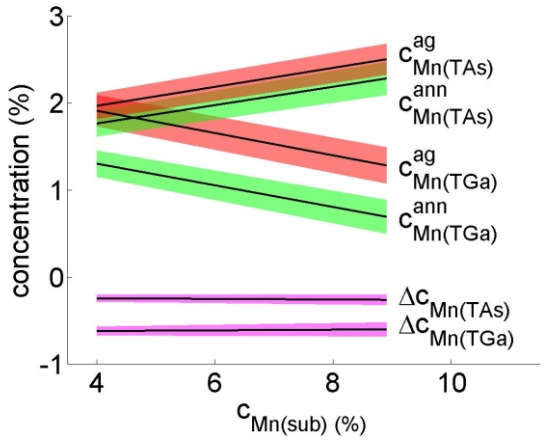

Figure 4. The fitting procedure was performed several times for several fixed substitutional Mn concentrations. The refined parameters giving the best fit of the measured and simulated data for as-grown (ag) and annealed (ann) sample are scattered along the straight lines. The concentrations of the interstitials in particular nonequivalent positions can be expressed as a function of fixed $c_{Mn(sub)}$. The coloured areas around the lines correspond to uncertainties in the linear regression of the fitting procedure results; the inaccuracy of the measurement is also included. The changes of the concentrations of the interstitials $c_{Mn(TAs)}$ and $c_{Mn(TGa)}$ after annealing are not dependent strongly on the fixed $c_{Mn(sub)}$.

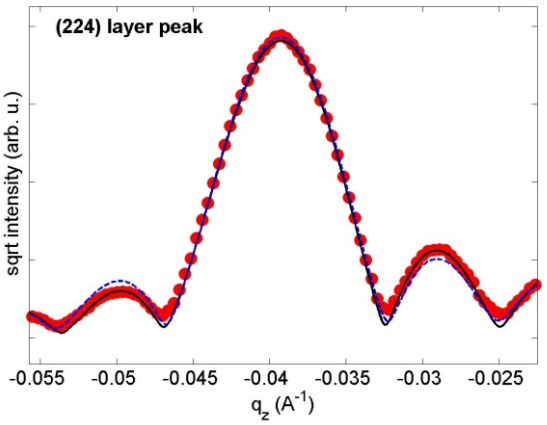

Figure 5. The diffraction maximum of the layer is plotted in detail; here the measured data are represented by circles. The diffraction curve simulated using the bilayer model (solid line) fits better the experimental data than the single-layer model (dashed), since it reproduces correctly the asymmetry of the measured curve.

Surprisingly, the diffraction curves for the last sample, which was sequentially etched and annealed, exhibits the asymmetry in the intensities of the side layer maxima (thickness fringes). It was not possible to reconstruct this asymmetry by different value of the structure factor. Considering the lateral homogeneity (previously checked), we explain this effect by vertical inhomogeneity. When we extended our model from homogenous single layer to model of two (Ga,Mn)As layers with different densities of interstitials, we were able to find better agreement of the simulated diffraction curves and experimental data (figure 5). This result clearly indicates the decrease of interstitials with decreasing depth below the surface. The combination of etching (i.e., releasing of model surface container) and short-time annealing kept the oxidizing rate of subsurface interstitials high (i.e., high flux of interstitials to the container), there was not enough time to saturate the surface container and later to homogenise the (Ga,Mn)As layer.

Observing this asymmetry we have determined the depth profiles of the interstitial density for all samples (actually, the as-grown and the annealed sample were homogenous) and these have been compared to the numerical simulations of the interstitial drift-diffusion in the sample. From this comparison the diffusivity of the interstitials in (Ga,Mn)As host lattice can be estimated (figure 6). This estimation can be done only with the precision of one order of magnitude, as there is some uncertainty in the concentration determination, consequently in the starting point of simulation, and finally, in the resulting XRD profile compared with the simulation. Nevertheless, the drift-diffusion simulations, whose solution is consistent with HRXRD results, showed the non-negligible contribution of internal electric field to the movement of the interstitials and its responsibility for self-homogenising of the (Ga,Mn)As layer during the annealing.

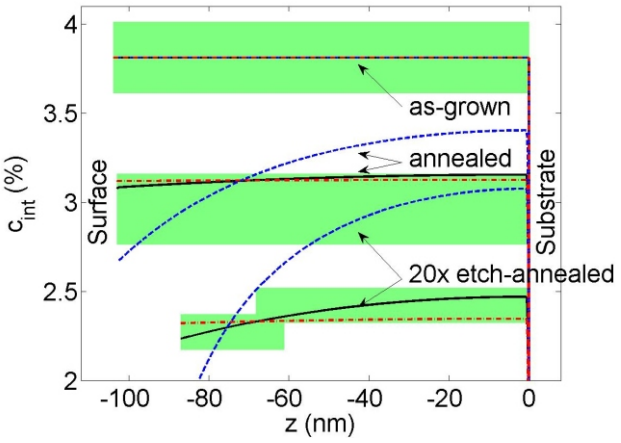

Figure 6. Depth profiles of the concentration of the Mn interstitials in as-grown sample, annealed and 20x etch-anneled. The concentration profiles determined by HRXRD are represented by green areas indicating the uncertainty of the profiles. The profiles obtained from the diffusion simulations for the interstitial diffusion constant $D_n = 4 \times 10^{-20}$ m^2/s are plotted by solid black lines; the concentration profiles simulated for 10 times larger and 10 times smaller values of the Mn diffusion constant are plotted by red and blue dashed lines, respectively. The initial concentration profile for all simulations is given by the concentration of Mn interstitials in as-grown sample.

Conclusion

We showed a strategy for the determination of the Mn interstitial concentration in (Ga,Mn)As epitaxial layers using high resolution X-ray diffractometry. The main idea was to measure diffraction curves around several diffraction maxima for different annealing states of the sample. All acquired data were simultaneously fitted to the theoretical curves. The method was demonstrated on the (Ga,Mn)As sample in several annealing steps: the as-grown state, then after 24 hours of annealing in the air at 160°C and finally after 20 cycles of etching and short annealing. The sample in all annealed states were measured and the interstitial densities and their changes due to the annealing were determined. The asymmetry of the intensities of the thickness fringes allows to characterize an eventual depth inhomogeneity of the interstitial density in the (Ga,Mn)As layer. This depth profile was approximated by the step-like function (actually two homogenous sublayers). Although the smooth function would correspond better to the exact profile, it is not possible to use it due to the large number of parameters to fit. The diffusion process during the annealing can be modelled by the solving the system of the drift-diffusion equations. The comparisons of the determined depth profiles of the interstitials and the drift-diffusion simulations allowed to estimate the diffusivity of the Mn ions in the (Ga,Mn)As lattice at least in order of magnitude. The results show that the flux of the Mn ions towards the free surface is strongly affected by the internal electric field produced by inhomogeneously distributed holes.

References

1. Jungwirth T *et al, Phys. Rev.* B **72** 165204 (2005).
2. K. W. Edmonds, P. Boguslawski, K. Y. Wang, R. P. Campion, S. N. Novikov, N. R. S. Farley, B. L. Gallagher, C. T. Foxon, M. Sawicki, T. Dietl, M. Buongiorno Nardelli, and J. Bernholc, *Phys. Rev. Lett.* **92**, 037201 (2004).
3. J. Adell, I. Ulfat, L. Ilver, J. Sadowski, K. Karlsson, and J. Kanski, *Journal of Physics Condensed Ma*tter **23**, 085003 (2011).
4. J. Mašek and F. Máca *Phys. Rev.* B **69** 165212 (2004).
5. L. Horák, Z. Šobáň, and V. Holý, *Journal of Physics: Condensed Matter* **22**, 296009 (2010).
6. F. Máca and J. Mašek, *Phys. Rev. B* **65**, 235209 (2002).
7. K. Olejník, V. Novák, M. Cukr, O. Pacherová, Z. Matěj, V. Holý, and M. Maryško, *AIP Conference Proceedings* **893**, 1219 (2007).
8. K. Olejník, M. H. S. Owen, V. Novák, J. Mašek, A. C. Irvine, J. Wunderlich, and T. Jungwirth, *Phys. Rev. B* **78**, 054403 (2008).
9. L. Horák, J. Matějová, X. Martí, V. Holý, V. Novák, Z. Šobáň, S. Mangold, and F. Jiménez-Villacorta, *Phys. Rev. B* **83**, 245209 (2011).
10. U. Pietsch, V. Holý and T. Baumbach *High-Resolution X-Ray Scattering from Thin Films and Lateral Nanostructures* (2004 Berlin: Springer) pp 97–121.
11. V. Holý, X. Martí, L. Horák, O. Caha, V. Novák, M. Cukr, and T. U. Schülli, *Applied Physics Letters* **97**, 181913 (2010).

Acknowledgements

This work is a part of the research programme MSM 0021620834 financed by the Ministry of Education of the Czech Republic. The work has been supported by the European Community's Seventh Framework Programme NAMASTE under grant agreement number 214499. The XANES experiment was carried out at synchrotron ANKA, Germany.